Inorganic Chemistry

Article

pubs.acs.org/IC

Increased Eu^{2+} Content and Codoping Mn^{2+} Induced Tunable Full-Color Emitting Phosphor $Ba_{1.55}Ca_{0.45}SiO_4:Eu^{2+},Mn^{2+}$

Shihai Miao,[†] Zhiguo Xia,*[,†,‡] Jie Zhang,[†] and Quanlin Liu[‡]

[†]School of Materials Sciences and Technology, China University of Geosciences, Beijing 100083, China

[‡]School of Materials Sciences and Engineering, University of Science and Technology Beijing, Beijing 100083, China

ABSTRACT: We demonstrated that a new intermediate composition of $Ba_{1.55}Ca_{0.45}SiO_4$ between the orthosilicates Ca_2SiO_4 and Ba_2SiO_4 yields the best phosphor hosts, and interesting luminescence properties can be found from the Eu^{2+} singly doped and/or Eu^{2+}/Mn^{2+} codoped $Ba_{1.55}Ca_{0.45}SiO_4$ phosphors. The phosphors can be excited by near-ultraviolet (nUV) light at wavelengths ranging from 200 to 450 nm matching well with the nUV light-emitting diode (LED) chips. As a result of fine-tuning the activators of different Eu^{2+} content and Eu^{2+}/Mn^{2+} couples with different ratios, tunable full-color emission under UV light excitation can be realized by combining the blue emission (460 nm) and green emission (520 nm) originating from Eu^{2+} with the red emission (595 nm) from Mn^{2+} in the $Ba_{1.55}Ca_{0.45}SiO_4$ host lattice. Energy-transfer efficiency between Eu^{2+} and Mn^{2+} increases and tunable emission can be obtained with increasing Mn^{2+} doping content. These results indicate that the $Ba_{1.55}Ca_{0.45}SiO_4:Eu^{2+},Mn^{2+}$ phosphor will have potential use in nUV chip pumped white LED devices.

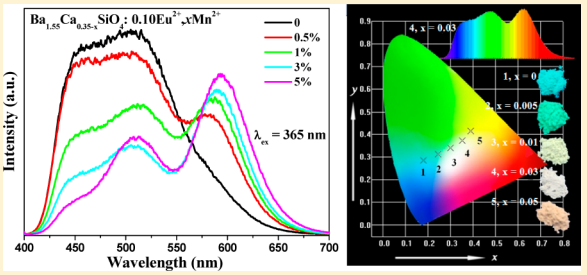

1. INTRODUCTION

In past decades, solid-state lighting technology has become commercially available with the rapid development of white light-emitting diodes (wLEDs) owing to the merits of being environmentally friendly, their long lifetime, energy-saving qualities, and high luminous efficiency.[1−3] At present, the most common method is to employ the yellow-emitting YAG:Ce^{3+} phosphor with blue InGaN chips to produce the practical white light emission. Unfortunately, the wLED based on the YAG:Ce^{3+} phosphor exhibits a high correlated color and low color rendering index (R_a < 80) because of the lack of a red component. Another alternative approach to achieve white light with high R_a and suitable T_c is the combination of a UV chip with red, green, and blue phosphors. However, the phosphor mixture produces an inevitable problem of fluorescence reabsorption between different phosphors and nonuniformity of luminescence properties, resulting in a loss of luminous efficiency and time-dependent shift of the color point. Therefore, it is essential to explore bright full-color red/green/blue-emitting phosphors for the development of tricolor emission phosphors upon near-UV (nUV) light.[4−6]

It is well-known that the alkaline earth silicate-based inorganic material is a kind of useful phosphor host, and it has been widely used in the lighting and display industry because of their stable crystal structures and flexible application properties. As an important class of alkaline earth silicate-based host, orthorhombic structure $M_2SiO_4:Eu^{2+}$ (M = Ca, Sr, and Ba) phosphors have been widely reported as commercial phosphors for wLED. Park reported the famous yellow phosphor $Sr_2SiO_4:Eu^{2+}$.[7] After that, as a phase composition modification strategy, Park reported the Ce^{3+}/Mn^{2+}-codoped and Eu^{2+}-doped T-phase $Ba_{1.2}Ca_{0.8}SiO_4$ phosphors for nUV wLEDs.[8] Yu reported the Eu^{2+} and Ce^{3+} codoped $SrCaSiO_4$ for wLEDs.[9] Fang et al. reported the blue-emitting $Ba_{1.3}Ca_{0.7}SiO_4:Eu^{2+}/Ce^{3+}$ phosphor.[10] Park studied the effect of Ba^{2+} substitution in Sr_3SiO_5 and proposed that low symmetry will be formed in the $(Sr,Ba)_3SiO_5$ solid−solution phase, and it will produce slight changes in the stacking arrangement of the cations, which in turn change the luminescence behaviors.[11] Very recently, Ram Seshadri's group studied the orthosilicate phosphors $Sr_xBa_{2-x}SiO_4:Eu^{2+}$, and they find that the intermediate compositions (x = 0.46), in which the two cation sites in the crystal structure are optimally bonded, yield the best luminescence properties.[12]

To the best of our knowledge, the luminescence properties of any activators in the $Ba_{1.55}Ca_{0.45}SiO_4$ host have not been reported up to now, and some interesting optical properties can be expected as the intermediate compositions in the orthorhombic M_2SiO_4 structure. Herein, we demonstrated a novel tunable single component white-light $Ba_{1.55}Ca_{0.45}SiO_4:Eu^{2+},Mn^{2+}$ phosphor for UV LEDs. We performed its phase structures and Eu^{2+} site preference analysis, and the Eu^{2+} content-dependent luminescent properties and energy transfer (ET) process between the Eu^{2+} and Mn^{2+} ions are discussed in detail. Besides, the emission color upon nUV light of as-prepared phosphors shifts from blue to green, to white, and even to red by varying the Eu^{2+} and Mn^{2+} content in this single host. The results indicate that the phosphors have potential for applications in the nUV pumped wLEDs lamps.

Received: June 20, 2014
Published: September 25, 2014

ACS Publications © 2014 American Chemical Society

2. EXPERIMENTAL SECTION

2.1. Materials and Synthesis. The designed $Ba_{1.55}Ca_{0.45-x-y}SiO_4:xEu^{2+},yMn^{2+}$ phosphors were synthesized by conventional high-temperature solid-state reaction. The starting materials were as follows: $BaCO_3$ (A.R.), $CaCO_3$ (A.R.), SiO_2 (A.R.), $MnCO_3$ (A.R.), Eu_2O_3 (99.99%). First, the starting materials were mixed and ground in an agate mortar for 15−20 min. Then, the mixture was transferred to a crucible and then sintered at 1250 °C for 4h in a CO reductive atmosphere. After that, we obtained the final phosphors for further measurements.

2.2. Characterization. The powder X-ray diffraction (XRD) measurements were conducted on a D8 Advance diffractometer (Bruker Corporation, Germany) operating at 40 kV and 40 mA with Cu Kα radiation (λ = 1.5406 Å), and the scanning rate was fixed at 4°/min. The photoluminescence (PL) and photoluminescence excitation (PLE) spectra were measured by a Hitachi F-4600 spectrophotometer equipped with a 150 W xenon lamp as the excitation source. The decay curves were recorded on a spectrofluorometer (HORIBA, JOBIN YVON FL3-21), and 370 nm pulse laser radiation (nano-LED) was used as the excitation source. Quantum efficiency was measured using the integrating sphere on the FLS920 fluorescence spectrophotometer (Edinburgh Instruments Ltd., U.K.).

3. RESULTS AND DISCUSSION

3.1. Phase Analysis. XRD patterns of all the as-prepared $Ba_{1.55}Ca_{0.45-x-y}SiO_4:xEu^{2+},yMn^{2+}$ phosphors were collected to verify the phase purity, and the representative samples of $Ba_{1.55}Ca_{0.35}SiO_4:0.10Eu^{2+}$ and $Ba_{1.55}Ca_{0.30}SiO_4:0.10Eu^{2+},0.05Mn^{2+}$ were shown in the phase determination. As is shown in Figure 1a, we can find that all the diffraction peaks of the selected samples can be indexed to the corresponding standard data for the orthorhombic phase of $Ba_{1.55}Ca_{0.45}SiO_4$ (JCPDS 17−930), suggesting that the prepared samples belong to the pure phase and that the doped ions produce an obvious effect on the phase structure. To further understand the preferred crystallographic positions of the Eu^{2+} ions in the $Ba_{1.55}Ca_{0.45}SiO_4$ host, we prepared the samples according to the compositions of $Ba_{1.55}Ca_{0.45-x}SiO_4:xEu^{2+}$ and $Ba_{1.55-x}Ca_{0.45}SiO_4:xEu^{2+}$ (x = 0, 0.01, 0.03, 0.05, 0.10, 0.15). It is found that the diffraction peaks in the selected region of 27−33° shift slightly to the lower angle side with concentration increase of Eu^{2+} in $Ba_{1.55}Ca_{0.45-x}SiO_4:xEu^{2+}$, as shown in Figure 1b. However, as a comparison, the diffraction peaks of $Ba_{1.55-x}Ca_{0.45}SiO_4:xEu^{2+}$ phosphors in Figure 1c do not move basically, and we can found some impurity in the vicinity of 28°, which verified that Eu^{2+} cannot incorporate Ba^{2+} sites successfully. Furthermore, the shift of the diffraction peaks toward the lower-angle side is related to the substitution of Ca^{2+} ions by larger Eu^{2+}, so that the doped ions can be completely incorporated into the $Ba_{1.55}Ca_{0.45}SiO_4$ host. Such a character can be explained by Bragg's equation, and the cell volume increased with the replacement of Ca^{2+} by Eu^{2+} in the present host.

3.2. Eu^{2+} Content-Dependent Photoluminescence Properties. As is shown in Figure 2a, the PLE and PL spectra of $Ba_{1.55}Ca_{0.44}SiO_4:0.01Eu^{2+}$ phosphor are investigated. The PLE spectrum monitored at 460 nm exhibits a broad band from 200 to 450 nm, which matched well with the nUV chip for wLED applications, and it indicates that this kind of phosphor can potentially be used. Although the wavelength at 365 nm cannot form the typical excitation peak, it can be commercially available, so that it is very interesting to investigate the luminescence properties of the phosphors upon this monitoring wavelength. The PL spectrum consists of an asymmetric broad

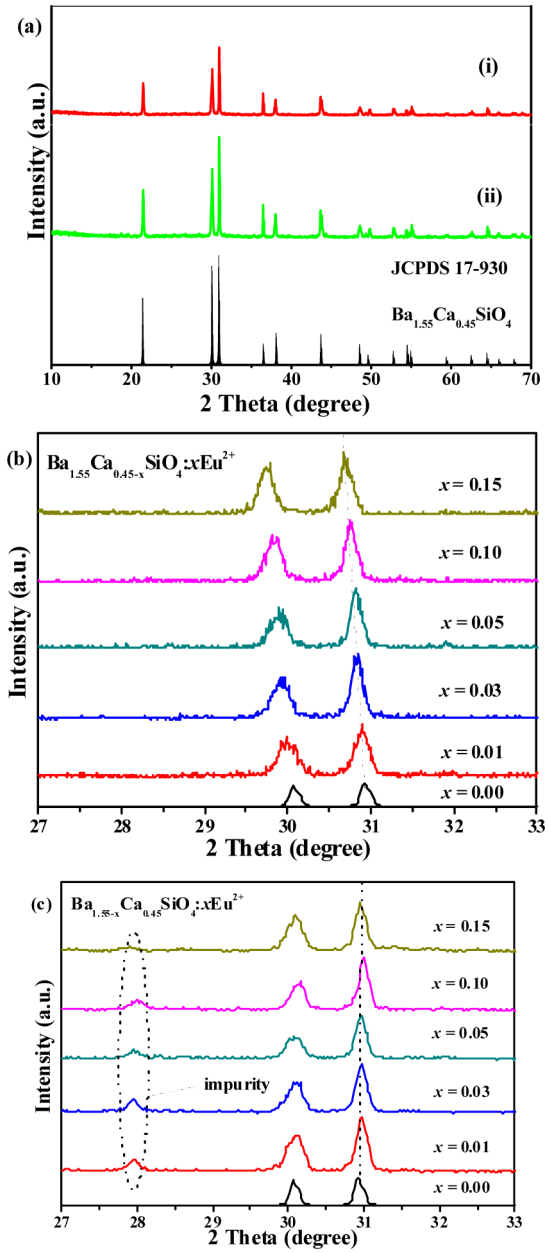

Figure 1. (a) XRD patterns of $Ba_{1.55}Ca_{0.35}SiO_4:0.10Eu^{2+}$ (i) and $Ba_{1.55}Ca_{0.30}SiO_4:0.10Eu^{2+},0.05Mn^{2+}$ (ii). The standard data for $Ba_{1.55}Ca_{0.45}SiO_4$ (JCPDS 17−930) is shown as a reference. (b) Magnified XRD patterns for $Ba_{1.55}Ca_{0.45-x}SiO_4:xEu^{2+}$ (x = 0, 0.01, 0.03, 0.05, 0.10, 0.15) phosphors. (c) Magnified XRD patterns for $Ba_{1.55-x}Ca_{0.45}SiO_4:xEu^{2+}$ (x = 0, 0.01, 0.03, 0.05, 0.10, 0.15) phosphors.

band centered at 460 nm under the excitation of 365 nm, which is ascribed to the electric dipole-allowed transition of the Eu^{2+} ions from the lowest level of the 5d excited state to the 4f ground state. Figure 2b gives the PL spectra of $Ba_{1.55}Ca_{0.45-x}SiO_4:xEu^{2+}$ (x = 0.01, 0.05, 0.10, 0.15, 0.20). Broad emission bands were clearly observed in the 400−700 nm range for all the samples with different Eu^{2+} content. From Figure 2b we can see that with increasing Eu^{2+} concentration, the PL demonstrates a broadening spectral profile, and the emission peaks give a red-shift. The emission peaks can shift from 460 to 520 nm and eventually to 550 nm. When Eu^{2+} concentration (x) is equal to 0.10, there are two equivalent emission bands (with maxima at 460 and 520 nm) upon 365

dx.doi.org/10.1021/ic501450f | Inorg. Chem. 2014, 53, 10386−10393

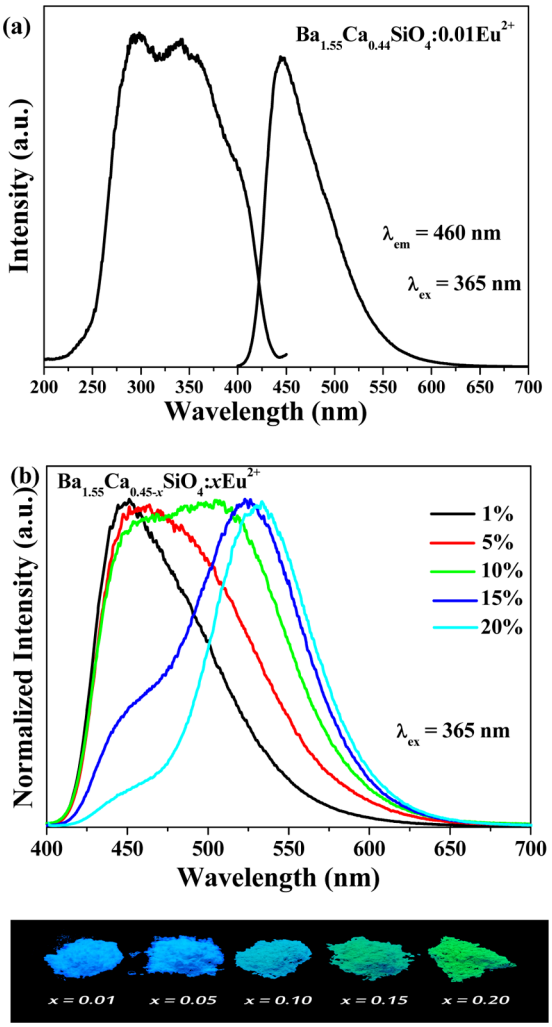

Figure 2. (a) PLE and PL spectra of $Ba_{1.55}Ca_{0.42}SiO_4$:0.03Eu^{2+}. (b) PL spectra of $Ba_{1.55}Ca_{0.45-x}SiO_4$:x$Eu^{2+}$ (x = 0.01, 0.05, 0.10, 0.15, and 0.20).

nm excitation. When Eu^{2+} concentration is increased from 0.10 to 0.20, this phenomenon is always there; the blue emission peak (460 nm) decreases, and the green peak (520 nm) increases with increasing Eu^{2+} content. In the bottom part of Figure 2, the digital photos of the $Ba_{1.55}Ca_{0.45-x}SiO_4$:x$Eu^{2+}$ phosphors under 365 nm UV lamp are shown, and we can clearly find the emission color evolution from blue to green with increasing Eu^{2+} doping content.

The above Eu^{2+} content-dependent two-peak emission behavior also indicates that there are two kinds of emission centers, which are in accordance with the two different types of crystallographic environment of Eu^{2+}.[13] Accordingly, Figure 3 shows the typical PLE (λ_{em} = 460 nm and λ_{em} = 520 nm) and PL (λ_{ex} = 365 nm) spectra of $Ba_{1.55}Ca_{0.35}SiO_4$:0.10Eu^{2+}. As a comparison, the PLE spectra for different monitoring wavelengths (λ_{em} = 460 nm and λ_{em} = 520 nm) have the similar broad band between 200 and 500 nm except for the intensities, which both correspond to the 4f−5d transition of Eu^{2+} ions. As is also found from the excitation spectrum monitoring by 460 and 520 nm in Figure 3, different spectral profiles indicated that the two emission peaks should be ascribed to two different Eu^{2+} emission centers. Furthermore, the PL spectrum could be divided into two Gaussian emission spectra at 460 and 520 nm,

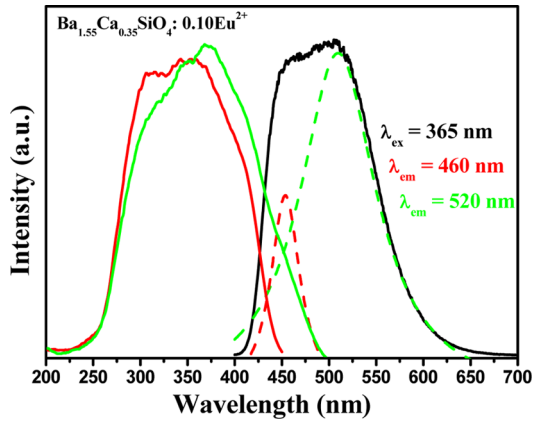

Figure 3. PLE (λ_{em} = 460 and 520 nm) and PL (λ_{ex} = 365 nm) spectra of $Ba_{1.55}Ca_{0.35}SiO_4$:0.10Eu^{2+}, and the Gaussian fit of the PL spectrum.

which verified the existence of the two different emission centers. Moreover, as we know, the broad-band emission peak in the visible region is beneficial for the general illumination of wLEDs.[5,14] So we choose the concentration of Eu^{2+} ion to be 0.10 for the design of color-tunable $Ba_{1.55}Ca_{0.35-x}SiO_4$:0.10$Eu^{2+}$,x$Mn^{2+}$ phosphor.

3.3. Photoluminescence Properties of Eu^{2+}/Mn^{2+} Codoped Samples. Figure 4a displays the PLE and PL

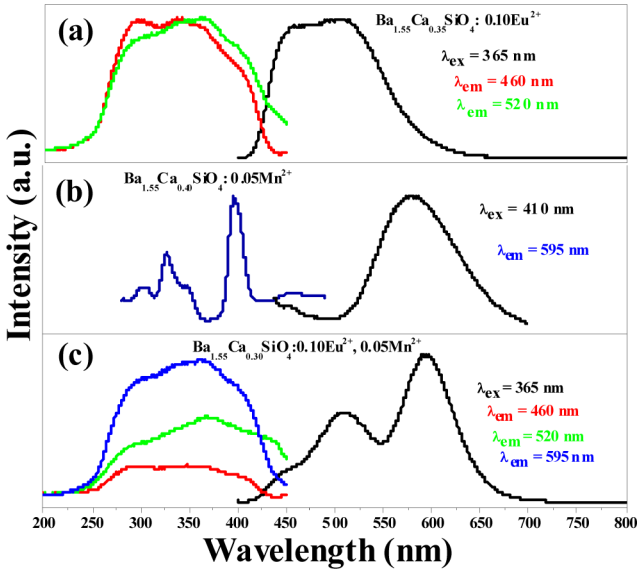

Figure 4. PLE (left) and PL (right) spectra of $Ba_{1.55}Ca_{0.35}SiO_4$:0.10Eu^{2+} (a), $Ba_{1.55}Ca_{0.40}SiO_4$:0.05Mn^{2+} (b), and $Ba_{1.55}Ca_{0.30}SiO_4$:0.10Eu^{2+},0.05Mn^{2+} (c).

spectra of Eu^{2+} singly doped $Ba_{1.55}Ca_{0.35}SiO_4$:0.10Eu^{2+} phosphor. The broad-band excitation and emission behaviors were discussed above. Figure 4b demonstrates the PL and PLE spectra of $Ba_{1.55}Ca_{0.40}SiO_4$:0.05Mn^{2+}. The excitation spectrum consists of several bands centering at 463, 410, 343, and 322 nm, corresponding to the transitions of Mn^{2+} ion from ground level $^4T_1(^4G)$, [$^4A_1(^4G)$, $^4E(^4G)$], $^4T_2(^4D)$, and $^6A_1(^6S)$ to$^4E(^4D)$levels, respectively. The broad emission band from 500 to 750 nm centered at 595 nm is ascribed to the spin-forbidden $^4T_1(^4G)$−$^6A_1(^6S)$ transition of the Mn^{2+} ions.[11,15] On the basis of the comparison of the PLE and PL spectra in Figure 4a,b, it is found that there is a spectral overlap between

dx.doi.org/10.1021/ic501450f | Inorg. Chem. 2014, 53, 10386−10393

the PL spectrum of Eu^{2+} and PLE spectrum of Mn^{2+}. Then, the ET from Eu^{2+} to Mn^{2+} ions is expected to happen in the $Ba_{1.55}Ca_{0.45}SiO_4$ system. To confirm the phenomenon, Figure 4c illustrates the PLE and PL spectra of the $Ba_{1.55}Ca_{0.30}SiO_4$:0.10Eu^{2+},0.05Mn^{2+} phosphors. It is also found that the excitation spectrum of $Ba_{1.55}Ca_{0.30}SiO_4$:0.10Eu^{2+},0.05Mn^{2+} monitored upon 460 and 520 nm (Eu^{2+} emission) is similar to the spectrum monitored upon 595 nm (Mn^{2+} emission) except for the different intensity suggesting an evidence on the ET from Eu^{2+} to Mn^{2+}. After codoping Eu^{2+} and Mn^{2+} ions in the $Ba_{1.55}Ca_{0.45}SiO_4$ host, the PL spectrum exhibits a broad emission, which includes the blue and green emission bands corresponding to the allowed f−d transition of the Eu^{2+} ions and an intense red emission band assigned to the forbidden transition of the Mn^{2+} ions. The emission spectrum of $Ba_{1.55}Ca_{0.30}SiO_4$:0.10Eu^{2+},0.05Mn^{2+} nearly covers the whole visible region. Therefore, tunable full-color emission, even the white-light emission, can be obtained by mixing the emission of the Eu^{2+} and Mn^{2+} ions in a single host lattice with simply adjusting the amounts of the activators via the principle of energy transfer.[16−19]

Therefore, a series of samples with fixed Eu^{2+} content and variable Mn^{2+} content were prepared to study the doping concentration-dependent luminescence properties of the phosphors. The PL spectra of $Ba_{1.55}Ca_{0.35-x}SiO_4$:0.10$Eu^{2+}$,x$Mn^{2+}$ (x = 0−0.05) phosphors upon the excitation of 365 nm are depicted in Figure 5. Considering the previous

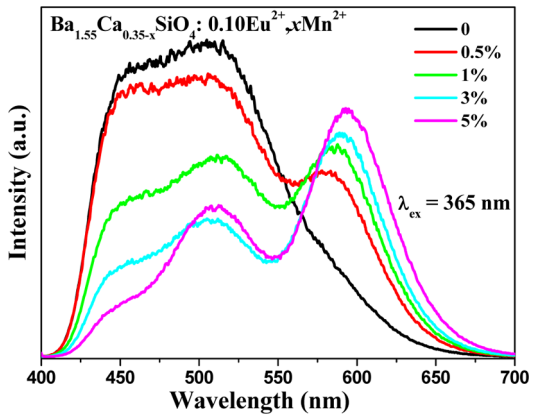

Figure 5. PL spectra of $Ba_{1.55}Ca_{0.35-x}SiO_4$:0.10$Eu^{2+}$,x$Mn^{2+}$ (x = 0, 0.005, 0.01, 0.03, 0.05) phosphors under 365 nm excitation.

analysis, the Eu^{2+} concentration was fixed at 0.10, while the content of Mn^{2+} is changed. As a result of fine-tuning the emission composition of the Eu^{2+} and Mn^{2+} ions, white-light emission can be realized by combining the emission of Eu^{2+} and Mn^{2+} in a single $Ba_{1.55}Ca_{0.45}SiO_4$ host lattice.[6] Therefore, the emission intensities at 460 and 520 nm, which are both ascribed to Eu^{2+} ions, decreased; however, the Mn^{2+} red emission at about 590 nm increased with increasing Mn^{2+} content. Furthermore, a red-shift behavior originating from Mn^{2+} ions can also be observed with increasing Mn^{2+} content. The peak wavelength positions are located at ∼582 nm at x = 0.005 and 593 nm at x = 0.05, which could be ascribed to the variation of crystal field strength. Herein, the crystal field around Mn^{2+} is proposed to obey

$$D_q = \frac{ze^2r^4}{6R^5} \quad (1)$$

where D_q is measurement of the crystal field strength, z is the charge or valence of the anion, R is the distance between the central ion and its ligands, r is the radius of the d wave function, and e is the charge of an electron. When Mn^{2+} ion was introduced into the $Ba_{1.55}Ca_{0.45}SiO_4$ host, the lattice constants for both V and a would decrease since the ionic radius of the doped Mn^{2+} is smaller than that of the Ca^{2+} ion, which would in turn lead to the increase of crystal field strength surrounding Mn^{2+} ions. Therefore, a larger crystal field splitting of 3d energy level originating from Mn^{2+} appears, and this makes the lowest 3d state of Mn^{2+} close to its ground state; finally, the PL emission peak of the Mn^{2+} ion performs a red-shift behavior. Moreover, it is accepted that the difference of chemical environment around Mn^{2+} may also be contributing to the observed red shift.[19−21]

The crystal distance R_c among the activators can be calculated by using the concentration quenching method, and it is given below.

$$R_c \approx 2\left(\frac{3V}{4\pi x_c N}\right)^{1/3} \quad (2)$$

where x_c is the concentration of activator at which the quenching occurs; N is the number of cations in the single unit cell, and V is the volume of the unit cell. For $Ba_{1.55}Ca_{0.45}SiO_4$ host lattice, N = 4, V = 419.37 Å^3, and x_c is 0.15 denotes the sum of Eu^{2+} concentration of 0.10 and the critical Mn^{2+} concentration of 0.05. The critical distance R_c is determined to be 15.8 Å, showing the ET mechanism in this system is governed by multipolar interaction.[21]

On the basis of Dexter's formula of multipolar interaction, we can obtain the following relation:

$$\frac{I_{S0}}{I_S} \propto C^{n/3} \quad (3)$$

where I_{s0} and I_s are the luminescence intensities of the sensitizer Eu^{2+} with and without the activator Mn^{2+}, and C is the concentration of the sum of Eu^{2+} and Mn^{2+}. The plots of (I_{s0}/I_s) versus $C^{n/3}$ with n = 6, 8, and 10 correspond to dipole−dipole (d−d), dipole−quadrupole (d−q), and quadrupole−quadrupole (q−q) interactions, respectively. The relationships between (I_{s0}/I_s) versus $C^{n/3}$ are illustrated in Figure 6, and a linear behavior was observed only when n = 10. This clearly indicates that the ET from Eu^{2+} to Mn^{2+} follows a quadrupole−quadrupole interaction.[22]

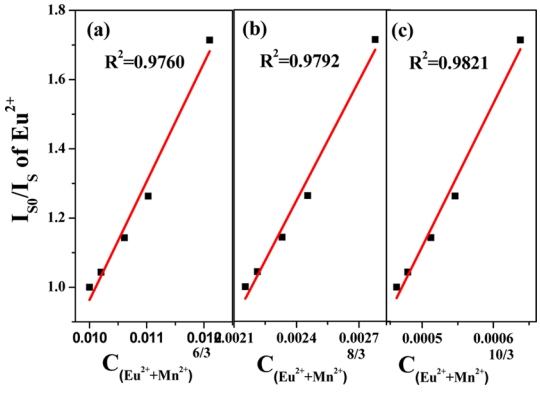

Figure 6. Dependence of I_{s0}/I_s of Eu^{2+} on (a) $C^{6/3}$, (b) $C^{8/3}$, and (c) $C^{10/3}$.

dx.doi.org/10.1021/ic501450f | Inorg. Chem. 2014, 53, 10386−10393

Figure 7a shows the powder diffuse reflectance spectrum (DRS) of the host, Eu^{2+} singly doped, and Eu^{2+},Mn^{2+} codoped

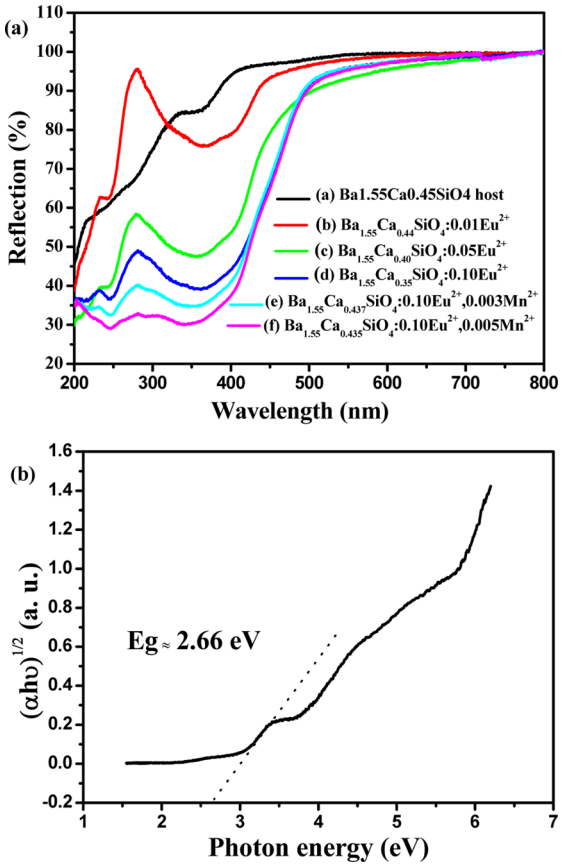

Figure 7. Powder DRS of $Ba_{1.55}Ca_{0.45}SiO_4$, $Ba_{1.55}Ca_{0.45-x}SiO_4$:$xEu^{2+}$ and $Ba_{1.55}Ca_{0.35-x}SiO_4$:$0.10Eu^{2+}$,$xMn^{2+}$ (a) and the band gap calculation of the $Ba_{1.55}Ca_{0.45}SiO_4$ host (b).

samples, respectively. The $Ba_{1.55}Ca_{0.45}SiO_4$ host shows a plateau of high reflection in the wavelength range of 360−800 nm and then starts to decrease dramatically from 360 to 200 nm, due to the host absorption. When Eu^{2+} ion is singly doped into the host, a broad band appears between 200 to 400 nm, which is assigned to the 4f−5d absorption of the Eu^{2+} ions. The absorption edge gradually shifts to longer wavelengths, and the absorption is enhanced at higher Eu^{2+} ions concentrations. For $Ba_{1.55}Ca_{0.35-x}SiO_4$:$0.10Eu^{2+}$,$xMn^{2+}$, a similar spectrum is observed. Mn^{2+} ions may also contribute to the increased absorption intensity in the wavelength range from 200 to 450 nm by means of the metal−ligand charge transfer band of Mn^{2+}−O^{2-}. The broad absorption profiles of the Eu^{2+} singly doped and Eu^{2+}, Mn^{2+} codoped $Ba_{1.55}Ca_{0.45}SiO_4$ phosphors further verified that these kind of phosphors can be used in the nUV pumped wLEDs.

The band gap of the $Ba_{1.55}Ca_{0.45}SiO_4$ host is further shown in Figure 7b. The band gap of the $Ba_{1.55}Ca_{0.45}SiO_4$ host can be estimated according to eq 4:[23]

$$[F(R_\infty)h\nu]^n = A(h\nu - E_g) \tag{4}$$

where $h\nu$ is the photon energy, E_g is the value of the band gap, A is a proportional constant, $n = 2$ for a direct transition or 1/2 for an indirect transition, and $F(R_\infty)$ is a Kubelka−Munk function defined as

$$F(R_\infty) = (1 - R)^2/2R = K/S \tag{5}$$

where R, K, and S are the reflection, the absorption coefficient, and the scattering coefficient, respectively. From the linear extrapolation of $[F(R_\infty)h\nu)^{1/2}] = 0$, the E_g value was estimated to be ∼2.66ev.

3.4. Energy-Transfer Study of Eu^{2+}/Mn^{2+} Codoped Samples. In the present $Ba_{1.55}Ca_{0.35-x}SiO_4$:$0.10Eu^{2+}$,$xMn^{2+}$ (x = 0−0.05) phosphors, the ET efficiency (η_T) from a sensitizer Eu^{2+} to an activator Mn^{2+} can be calculated via eq 6:

$$\eta_T = 1 - \frac{I_s}{I_{s0}} \tag{6}$$

where I_{s0} is the luminescence intensity of the sensitizer Eu^{2+} in the absence of Mn^{2+}, and I_s is the luminescence intensity of Eu^{2+} in the presence of Mn^{2+}. η_T is the ET efficiency from Eu^{2+} to Mn^{2+} in the present $Ba_{1.55}Ca_{0.35-x}SiO_4$:$0.10Eu^{2+}$,$xMn^{2+}$ (x = 0−0.05). As found from the spectral profiles in Figure 5, the ET efficiency from the sensitizer Eu^{2+} to the activator Mn^{2+} increases gradually with increasing Mn^{2+} doping concentration.[22,23] To better understand the ET behaviors between Eu^{2+} and Mn^{2+} and find the contribution of different emission centers of Eu^{2+} to Mn^{2+} emission, Figure 8a,b gives the fluorescence decay curves of Eu^{2+} emission by monitoring different emission centers corresponding to the wavelength at 460 and 520 nm in $Ba_{1.55}Ca_{0.35-x}SiO_4$:$0.10Eu^{2+}$,$xMn^{2+}$ (x = 0−0.05) phosphors. It is found that all the decay curves show a

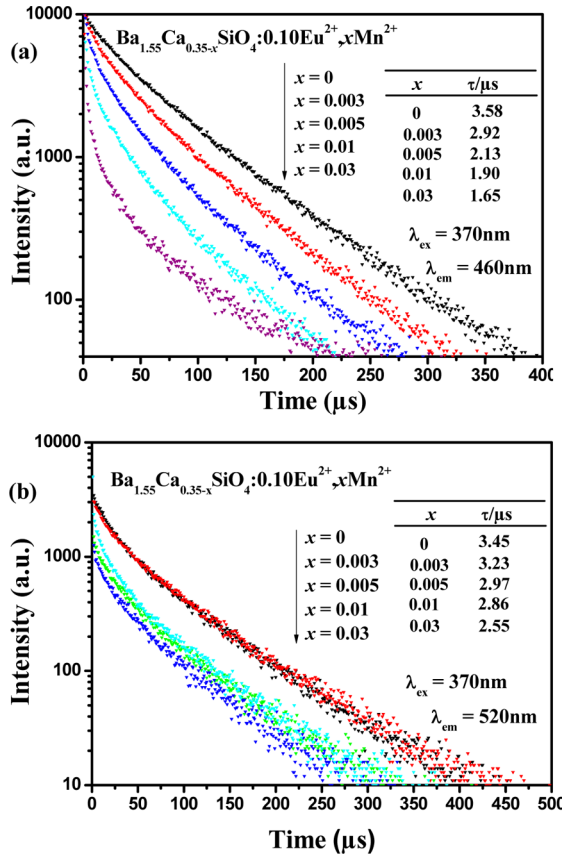

Figure 8. Decay curves of Eu^{2+} emission in $Ba_{1.55}Ca_{0.35-x}SiO_4$:$0.10Eu^{2+}$,$xMn^{2+}$ phosphors under excitation at 370 nm, monitored at 460 nm (a) and 520 nm (b).

dx.doi.org/10.1021/ic501450f | Inorg. Chem. 2014, 53, 10386−10393

second-order exponential decay, which can be fitted by the equation

$$I(t) = I_0 + A_1 \exp(-t/\tau_1) + A_2 \exp(-t/\tau_2) \quad (7)$$

where $I(t)$ is the luminescence intensity at time t, τ_1 and τ_2 are rapid and slow times for the exponential components, respectively, and A_1 and A_2 are constants.[24] The average lifetime τ^* can be obtained by the formula as follows:

$$\tau^* = (A_1\tau_1^2 + A_2\tau_2^2)/(A_1\tau_1 + A_2\tau_2) \quad (8)$$

The decay lifetimes at 460 nm were determined to be 3.58, 2.92, 2.13, 1.90, and 1.65 μs and 3.45, 3.23, 2.97, 2.86, and 2.55 μs for 520 nm with different Mn^{2+} doped concentrations. Obviously the decay times decreased monotonically as the Mn^{2+} concentration increased, which strongly demonstrated the ET from Eu^{2+} to Mn^{2+}. It is also found that the lifetime at 460 nm decreases more quickly than that at 520 nm, which means that the blue emission centers contribute more to the Mn^{2+} emission, and this is also in relation to the main spectral overlap between the blue emission centers and the exiction band of Mn^{2+}.

The ET efficiency η_T between the Eu^{2+} and Mn^{2+} ions was also obtained from the decay lifetime by using the equation

$$\eta_T = 1 - \frac{\tau_x}{\tau_0} \quad (9)$$

where the τ_x and τ_0 are the lifetimes of sensitizer (Eu^{2+}) ion with and without the activator (Mn^{2+}), respectively.[25,26] As shown in Figure 9, the lifetime values and ET efficiencies from two Eu^{2+} emission centers are plotted as a function of the Mn^{2+} concentration. One can find that the average lifetimes decrease monotonously, while the ET efficiency increases gradually with increasing Mn^{2+} content. The value of η_T reaches the maximum of 45.9% and 35.7% for the two emission centers monitored at 460 nm (a) and 520 nm (b) when n = 0.05, indicating that the energy transfer from the Eu^{2+} to Mn^{2+} is efficient.

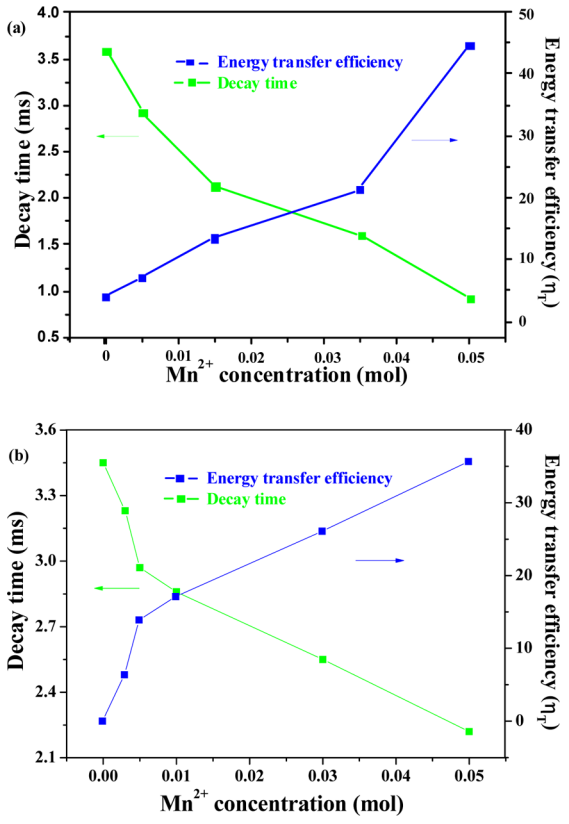

Figure 9. Dependence of the fluorescence lifetime of the Eu^{2+} and energy-transfer efficiency on doped Mn^{2+} molar concentration in $Ba_{1.55}Ca_{0.35-x}SiO_4$:0.10$Eu^{2+}$,$x$$Mn^{2+}$ samples, monitored at 460 nm (a) and 520 nm (b).

3.5. Quantum Efficiencies, CIE Chromaticity Coordinates, and Color Purity. We also measured the internal quantum efficiency (QE) of composition-optimized $Ba_{1.55}Ca_{0.35}SiO_4$:0.10Eu^{2+} phosphor. As given in Figure 10,

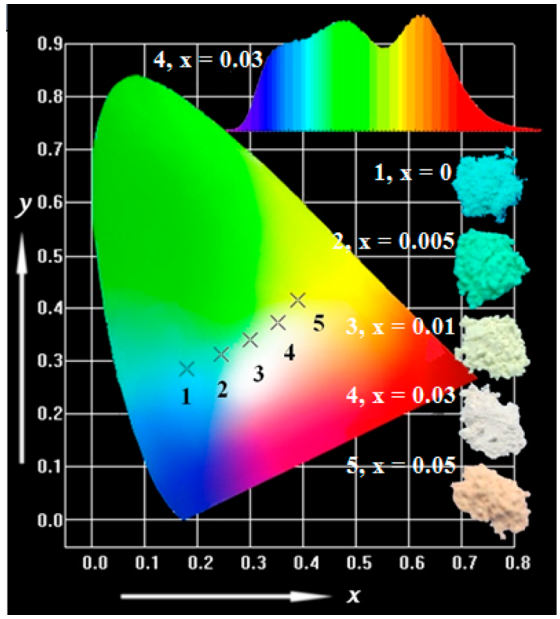

Figure 10. CIE chromaticity diagram and a series of digital photographs of the selected $Ba_{1.55}Ca_{0.35-x}SiO_4$:0.10$Eu^{2+}$,$x$$Mn^{2+}$ (x = 0, 0.005, 0.01, 0.03, 0.05) phosphors (λ_{ex} = 365 nm). (inset) The PL spectrum of $Ba_{1.55}Ca_{0.32}SiO_4$:0.10Eu^{2+},0.03Mn^{2+} under 365 nm UV lamp.

the internal QE value can be calculated by the following equation:

$$\eta_{QE} = \frac{\int L_S}{\int E_R - \int E_S} \quad (10)$$

where L_S is the emission spectrum of the studied sample, E_S is the spectrum of the light used for exciting the sample, and E_R is the spectrum of the excitation light without the sample in the sphere. All the spectra were measured by using the integrated sphere on the FLS920 fluorescence spectrophotometer. The measured internal QE value of $Ba_{1.55}Ca_{0.35}SiO_4$:0.10Eu^{2+} phosphor is determined as 44.73% under 410 nm excitation. The variation of the Commission International de L'Eclairage (CIE) chromaticity coordinates of the $Ba_{1.55}Ca_{0.35-x}SiO_4$:0.10$Eu^{2+}$,$x$$Mn^{2+}$ phosphors with different doping contents of Mn^{2+} are calculated based on the corresponding PL spectrum upon 365 nm excitation, and the results are summarized in Figure 11 and Table 1, respectively. It can be seen that the emitting color of the phosphors can be easily modulated from blue to green, to white and even to red, by simply varying the value of n from 0 to 0.05. Accordingly, the corresponding CIE coordinates of $Ba_{1.55}Ca_{0.35-x}$-

dx.doi.org/10.1021/ic501450f | Inorg. Chem. 2014, 53, 10386−10393

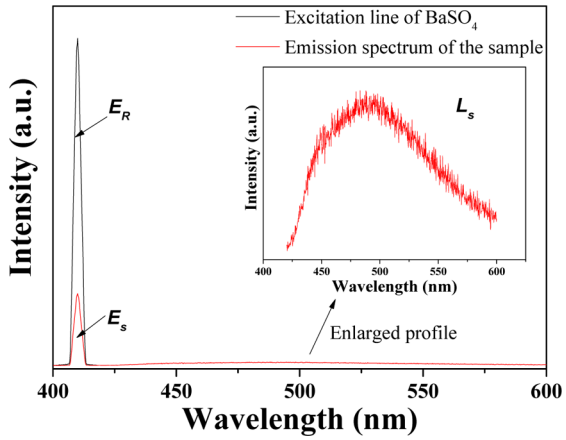

Figure 11. Excitation line of $BaSO_4$ and emission spectrum of $Ba_{1.55}Ca_{0.35}SiO_4$:0.10Eu^{2+} phosphor collected by using an integrating sphere. (inset) The magnification of the emission spectrum.

Table 1. Comparison of the CIE Chromaticity Coordinates (x, y) for $Ba_{1.55}Ca_{0.35-x}SiO_4$:0.10$Eu^{2+}$, xMn^{2+} (x = 0−0.05) Phosphors Excited at 365 nm

sample no.	sample composition (y)	CIE coordinates (x, y)
1	0	(0.181, 0.285)
2	0.005	(0.255, 0.335)
3	0.01	(0.298, 0.336)
4	0.03	(0.352, 0.373)
5	0.05	(0.390, 0.414)

SiO_4:0.10Eu^{2+},xMn^{2+} change from (0.181, 0.285) to (0.390, 0.414) due to the different emission composition of the Eu^{2+} and Mn^{2+} ions. Thus, the emission colors can be tunable in a large color gamut by changing the doping content of Mn^{2+} ions. Furthermore, the white-light emission with CIE coordinates of (0.352, 0.373) can be obtained by combining the emission of Eu^{2+} and Mn^{2+} in a single host. The color purity values of the selected samples were also studied in this study. The color purity of the phosphors with different color is the weighted average of the (x, y) coordinate relative to the coordinate of the CIE white illuminants and the coordinate of the dominant wavelength, which can calculated by the following equation:[27]

$$p = \sqrt{\frac{(x - x_i)^2 + (y - y_i)^2}{(x_d - x_i)^2 + (y_d - y_i)^2}} \quad (11)$$

where (x, y) and (x_i, y_i) are the color coordinates of the studied phosphors and the CIE illuminant (0.3101, 0.3162), respectively. (x_d, y_d) are the color coordinates of the dominant wavelength. In the present case, the CIE coordinates (x, y) of blue-greenish $Ba_{1.55}Ca_{0.35}SiO_4$:0.10Eu^{2+} and white $Ba_{1.55}Ca_{0.32}SiO_4$:0.10Eu^{2+},0.03Mn^{2+} phosphors are (0.181, 0.285) and (0.352, 0.373), respectively. The dominant wavelength is obtained by drawing a straight line from the illuminant (0.3101, 0.3162) to the (x, y) coordinates of the studied samples and by extending the straight line to the perimeter of the chromaticity diagram. The intersection point is the dominant wavelength of the samples, which are determined to be (0.05, 0.25) and (0.47, 0.52) for $Ba_{1.55}Ca_{0.35}SiO_4$:0.10Eu^{2+} and $Ba_{1.55}Ca_{0.32}SiO_4$:0.10Eu^{2+},0.03Mn^{2+}, respectively. On the basis of the above data, the color purity for the two typical samples were calculated to be 49.5% and 29.3%.

4. CONCLUSIONS

A novel single-phased white-light phosphor $Ba_{1.55}Ca_{0.45}SiO_4$:Eu^{2+},Mn^{2+} has been prepared by the traditional solid-state process. The pure phase structure and the crystallographic positions of the Eu^{2+} ions in the $Ba_{1.55}Ca_{0.45}SiO_4$ host were discussed from the XRD analysis. Eu^{2+} and Eu^{2+}/Mn^{2+} content-dependent photoluminescence properties have been discussed in detail. The critical distance of the Eu^{2+}/Mn^{2+} couples is calculated, and the concentration quenching mechanism is proven to be a quadrupole−quadrupole interaction. Energy-transfer efficiency between Eu^{2+} and Mn^{2+} increases and tunable emission can be obtained with an increase of the Mn^{2+} doping content. As a result of fine-tuning the activators of different Eu^{2+} content and Eu^{2+}/Mn^{2+} couples with different ratios, tunable full-color emission under UV light excitation can be realized by combining the blue emission (460 nm) and green emission (520 nm) originating from Eu^{2+} with the red emission (595 nm) from Mn^{2+} in a single $Ba_{1.55}Ca_{0.45}SiO_4$ host lattice. The above results indicate that the color-tunable $Ba_{1.55}Ca_{0.45}SiO_4$:Eu^{2+},Mn^{2+} phosphor has great potential for white light-emitting diode applications.

AUTHOR INFORMATION

Corresponding Author

*E-mail: xiazg@ustb.edu.cn (Z. Xia).

Notes

The authors declare no competing financial interest.

ACKNOWLEDGMENTS

The present work was supported by the National Natural Science Foundations of China (Grant Nos. 51002146 and 51272242), Natural Science Foundations of Beijing (2132050), the Program for New Century Excellent Talents in the University of the Ministry of Education of China (NCET-12-0950), Beijing Nova Program (Z131103000413047), Beijing Youth Excellent Talent Program (YETP0635), and the Funds of the State Key Laboratory of New Ceramics and Fine Processing, Tsinghua University (KF201306). Z.G.X. is also grateful for the financial support from University of Science and Technology Beijing.

REFERENCES

(1) Xia, Z. G.; Zhang, Y. Y.; Molokeev, M.; Atuchin, V. V.; Luo, Y. *Sci. Rep.* **2013**, *3*, 3310.
(2) Xia, Z. G.; Wang, X. M.; Wang, Y. X.; Liao, L. B.; Jing, X. P. *Inorg. Chem.* **2011**, *50*, 10134−10142.
(3) Mao, Z. Y.; Wang, D. J. *Inorg. Chem.* **2010**, *49*, 4922−4927.
(4) Sohn, K. S.; Park, D. H.; Cho, S. H.; Kwak, J. S.; Kim, J. S. *Chem. Mater.* **2006**, *18*, 1768−1772.
(5) Zhou, J.; Xia, Z. G.; Yang, M. X.; Shen, K. *J. Mater. Chem.* **2012**, *22*, 21935−21941.
(6) Wu, W. W.; Xia, Z. G. *RSC Adv.* **2013**, *3*, 6051−6057.
(7) Park, J. K.; Lim, M. A.; Kim, C. H.; Park, H. D.; Park, J. T.; Choi, S. Y. *Appl. Phys. Lett.* **2003**, *82*, 683−685.
(8) Park, K.; Lee, J.; Park, J.; Kim, L.; Kung, P.; Kim, S. M.; Kim, G. *J. Lumin.* **2010**, *130*, 2442−2445.
(9) Yu, H.; Lai, Y. W.; Gao, G. M.; Kong, L.; Li, G. H.; Gan, S. C.; Hong, G. Y. *J. Alloys Compd.* **2011**, *509*, 6635−6639.
(10) Fang, Y. F.; Li, L. K.; Chen, Y. B.; Wang, H. B.; Zeng, R. J. *J. Lumin.* **2013**, *6*, 17−21.
(11) Park, J. K.; Choi, K. J.; Yeon, J. H.; Lee, S. J.; Kim, C. H. *Appl. Phys. Lett.* **2006**, *88*, 043511−043511−3.

(12) Denault, K. A.; Brgoch, J.; Gaultois, M. W.; Mikhailovsky, A.; Petry, R.; Winkler, H.; DenBaars, S. P.; Seshadri, R. *Chem. Mater.* **2014**, *26*, 2275−2282.
(13) Tezuka, S.; Sato, Y.; Komukai, T.; Takatsuka, Y.; Kato, H.; Kakahana, M. *Appl. Phys. Express* **2013**, *6*, 072101−072104.
(14) Schipper, W. J.; Blasse, G.; Leblans, P. *Chem. Mater.* **1994**, *6*, 1784−1789.
(15) Le, F. H.; Wang, L. X.; Jia, W.; Jia, D. Z.; Bao, S. J. *J. Alloys Compd.* **2012**, *512*, 323−327.
(16) Hao, Z.; Zhang, J.; Zhang, X.; Sun, X.; Luo, Y.; Lu, S.; Wang, X. *J. Appl. Phys. Lett.* **2007**, *90*, 261113−261117.
(17) Blasse, G. *Philips Res. Rep.* **1969**, *24*, 131−144.
(18) Du, F. P.; Zhu, R.; Huang, Y. L.; Tao, Y.; Seo, H. J. *Dalton Trans.* **2011**, *40*, 11433−11437.
(19) Xia, Z. G.; Sun, J. F.; Du, H. Y.; Chen, D. M.; Sun, J. Y. *J. Mater. Sci.* **2010**, *45*, 1553−1559.
(20) Song, Z.; Liao, J.; Ding, X. L.; Zhou, T. L.; Liu, Q. L. *J. Lumin.* **2012**, *132*, 1768−1773.
(21) Chuang, H. Y.; Lu, C. H.; Hsu, C. H. *J. Am. Ceram. Soc.* **2010**, *93*, 1838−1841.
(22) Yang, J.; Zhang, C. M.; Li, C. X.; Lin, J. *Inorg. Chem.* **2008**, *47*, 7262−7270.
(23) Wang, J.; Wang, S. B.; Su, Q. *J. Solid State Chem.* **2004**, *177*, 895−900.
(24) Xie, R. J.; Hirosaki, N.; Kimura, N.; Sakuma, K.; Mitomo, M. *Appl. Phys. Lett.* **2007**, *90*, 191101−191103.
(25) Hou, Z. Y.; Wang, L. L.; Lian, H. Z.; Chai, R. T.; Zhang, C. M.; Cheng, Z. Y.; Lin, J. *J. Solid State Chem.* **2009**, *182*, 698−708.
(26) Yang, W. J.; Chen, T. M. *Appl. Phys. Lett.* **2006**, *88*, 101903−101905.
(27) Schubert, E. F. *Light Emitting Diodes,* 2nd ed.; Cambridge University Press: Cambridge, U.K., 2006.